Near-Field Radiation from a Ridge Waveguide Transducer in the Vicinity of a Solid Immersion Lens

Kürşat Şendur,* Chubing Peng, and William Challener
Seagate Technology Research Center, Pittsburgh, Pennsylvania 15222-4215 USA
(Received 15 June 2004; published 31 January 2005)

A near-field optical system is investigated to improve the transmission efficiency of near-field transducers. A ridge waveguide is placed adjacent to a solid immersion lens (SIL) but separated by a low-index dielectric layer. The incident electric field near the focus of the SIL is determined by the Richards-Wolf vector field equations. The finite element method is used to solve Maxwell's equations. A spot size of 31 nm is obtained. The maximum value of the absorbed optical power density in the recording medium is 7.51×10^{-4} mW/nm^3 for a 100 mW input power.

DOI: 10.1103/PhysRevLett.94.043901 PACS numbers: 42.79.Gn

There has been an increasing interest in generating intense optical spots smaller than the diffraction limit of an objective lens [1–5]. In addition to near-field imaging [2], intense subwavelength optical spots have potential applications in lithography and biochemical sensing. Near-field techniques that enhance localized surface plasmons are potential candidates to obtain intense optical spots beyond the diffraction limit for optical data storage. The magnetic storage industry is also interested in subwavelength optical spots for heat assisted magnetic recording [6] to overcome the superparamagnetic limit [7].

The ridge waveguide transducer (RWT), shown in Fig. 1, has been suggested as a near-field aperture for data storage [8]. Various RWT designs have been investigated [9–13] using electromagnetic modeling techniques, including the finite difference time domain (FDTD) and finite element method (FEM). Models for a focused beam of light were integrated with the FEM [13] and FDTD [14] for more realistic scenarios.

The focused spot size that can be obtained from a lens is proportional to the wavelength, and inversely proportional to the numerical aperture (NA) of the lens. The spot size can be reduced by increasing the index of refraction of the medium in which the light is focused, which increases the NA of the lens. Solid immersion lenses (SIL) [1], in which the light is focused in a high refractive index solid, achieve smaller optical spots than the conventional diffraction limit of air-spaced objective lenses. Increasing the NA using a SIL increases the electric field at the focal region. Figure 2 illustrates the maximum electric field produced at the focus of an optical system as a function of NA for linear polarization. The wavelength is 700 nm, and the optical power is 100 mW. Placing a near-field transducer in the proximity of such enhanced electric fields increases the near-field radiation from the transducer as well. In this Letter we discuss the near-field radiation of an optical system which is composed of a RWT placed in the vicinity of a SIL as shown in Fig. 3.

Surface plasmon modes can be optically excited in a metal film using the Otto [15] excitation technique in which light is incident from a high refractive index material onto the metal film via a thin low-index dielectric spacer. Because of the total internal reflection at the high-low-index boundary, evanescent waves are created which couple efficiently into the surface plasmon modes over the metal film. By placing a low-index material between the SIL and RWT as shown in Fig. 3, a similar effect is obtained. The presence of the thin layer with a low-dielectric index in Fig. 3 is further discussed in the results section.

In a previous study [13], a Gaussian beam approximation was used to model the interaction of focused light with near-field transducers. The near-field radiation from a RWT placed at the focus of an objective lens was investigated. The near-field radiation was expressed in terms of power density, which provided a better insight than the commonly used electric field enhancement. Focused light has a broad **k** spectrum, depending on the NA of the optical system. On the other hand, a plane wave is represented with a single point on the **k** spectrum. The interaction of near-field transducers, such as the RWT, with various components of the broad **k** spectrum is not adequately described by a single plane wave or a small number of plane waves without the proper weighting factors.

A focused beam model for a low NA objective has been previously considered [13]. To obtain larger field amplitudes at the near-field transducer, it can be placed at the focal point of a SIL. However, the model previously considered [13] is inadequate for objectives with large NAs.

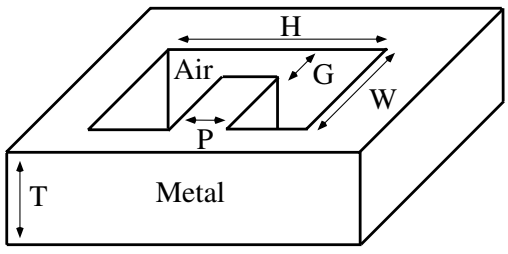

FIG. 1. The ridge waveguide transducer.

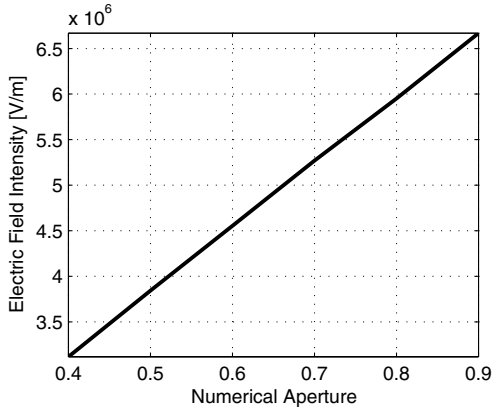

FIG. 2. Electric field magnitude at the focus of an optical system as a function of NA.

Richards and Wolf developed a method for calculating the electric field semianalytically near the focus of an aplanatic lens [16,17]. The total electric field in the neighborhood of the focus is given by

$$\mathbf{E}(\mathbf{r}_p) = -\frac{i}{\lambda}\int_0^{\alpha} d\theta \sin\theta \int_0^{2\pi} d\phi\, \mathbf{a}(\theta, \phi) \times \sqrt{\cos\theta}\exp(-i\mathbf{k}\cdot\mathbf{r}_p), \quad (1)$$

where α is the half angle of the beam, $\mathbf{r}_p$ is the observation point, $\mathbf{k}$ is the propagation vector, λ is the wavelength in the medium, $r_p = \sqrt{x_p^2 + y_p^2}$, and $\phi_p = \arctan(y_p/x_p)$. In Eq. (1), $\mathbf{a}(\theta, \phi)$ is the weighting vector for a plane wave incident from the (θ, ϕ) direction. $\mathbf{a}(\theta, \phi)$ is a polarization dependent quantity, and it can be written as

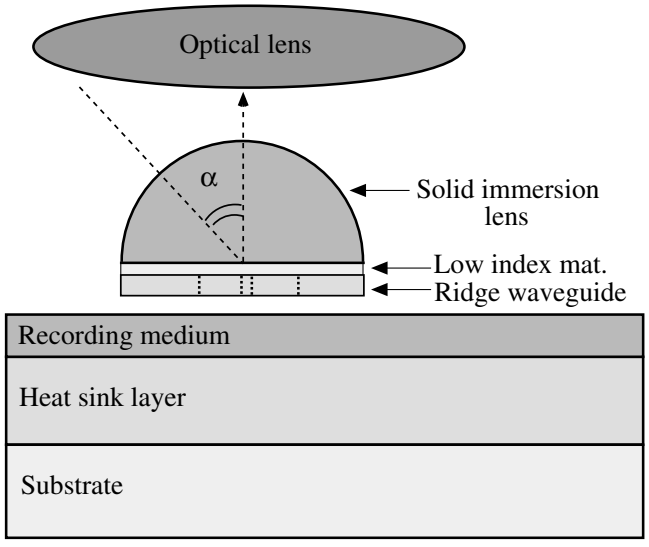

FIG. 3. Ridge waveguide is placed in the vicinity of a SIL. A low-dielectric index material is placed between the ridge waveguide and the SIL.

$$\mathbf{a}(\theta_i, \phi_j) = \begin{bmatrix} \cos\theta_i\cos^2\phi_j + \sin^2\phi_j \\ \cos\theta_i\cos\phi_j\sin\phi_j - \cos\phi_j\sin\phi_j \\ \sin\theta_j\cos\phi_j \end{bmatrix}, \quad (2)$$

for linear polarization. In Eq. (1), the $\sqrt{\cos\theta}$ factor is applied to the incident beam for energy conservation in a SIL, but no other apodization is applied.

Equation (1) can be viewed as a summation of plane waves propagating in the $\mathbf{k}$ direction with an amplitude of $-\frac{i}{\lambda}\sin\theta\sqrt{\cos\theta}$. Equation (1) is integrated with the FEM solver [18]. A reference solution is desired to validate the FEM solution in the case of a focused beam excitation, which is defined by the Richards-Wolf equations. Below we provide a summary of our model validation effort. We developed an analytical model to calculate the interaction of spherical particles with the focused fields calculated from the Richards-Wolf equations. Figure 4 illustrates the scattering from a spherical nanoparticle with a 250 nm radius in free space. The dielectric index of the particle is 2, and it is illuminated with the focused beam defined by Eq. (1). The half angle of the beam is 60°, and the operational wavelength is 700 nm. In Fig. 4, the total (incident + scattered) $|\mathbf{E}|^2$ is plotted on the $\hat{x}$-$\hat{z}$ plane. The FEM shows good agreement with the analytical model.

Using the FEM, we investigated the optical system given in Fig. 3. Based on a previous study [13], the RWT parameters are selected as $H = 218$ nm, $W = 38$ nm, $T = 64$ nm, $P = 19$ nm, and $G = 20$ nm. The operational wavelength is 516 nm. Silver, cobalt, and gold are used for the RWT, magnetic layer, and heat-sink layer, respectively. The refractive indices of the materials in this study are taken from the literature [19] as $0.130 + i \times 3.063$, $1.952 + i \times 3.654$, and $0.617 + i \times 2.111$ for silver, cobalt, and gold, respectively. Air, $n = 1$, is used as the low-index material. Figure 5 shows the maximum power density in the recording medium for different air thicknesses. The results suggest that the optimum coupling of near-field radiation from the RWT is obtained when the air thickness

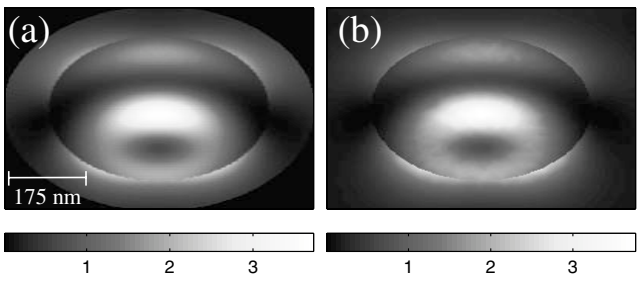

FIG. 4. Interaction of a linearly polarized focused beam with a dielectric sphere with a 250 nm radius. Dielectric index of the sphere is 2, and the wavelength is 700 nm. The total (incident + scattered) electric field is plotted on the $\hat{x}$-$\hat{z}$ plane. (a) Analytical solution, and (b) FEM solution.

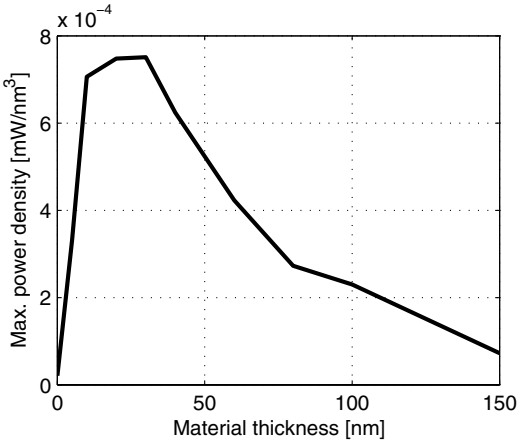

FIG. 5. Maximum power dissipation in the recording medium for various RWT-SIL separations.

is 30 nm. The presence of air creates evanescent waves, which couple efficiently into the surface plasmon modes over the metal film, similar to the Otto [15] excitation technique. This is the main reason for the enhancement in near-field radiation. Moreover, the spot size does not change significantly for different L. The spot size depends on the RWT geometry, including the distance between the ridge and opposite waveguide wall, and is not affected by the thickness of the other layers. Figure 6 illustrates the dissipated power density on the top surface of the recording medium for $L = 30$ nm. The FWHM spot diameter in the recording medium is 31 nm, and the maximum absorbed power density is about 7.51×10^{-4} mW/nm^3 for a 100 mW input power. The power density mentioned above is about 4.5 times higher than the previously calculated 1.67×10^{-4} mW/nm^3 when the RWT was placed at the focus of an objective lens [13]. For a bit-aspect ratio of 1, these numbers provide an areal density on the order of 660 Gb/in^2. With a higher bit-aspect ratio, a better recording medium design, and a disregard for the manufacturing challenges, the aforementioned power density and spot diameter can yield 4 Tb/in^2. Currently, state of the art recording devices have an areal density around 90 Gb/in^2, whereas the recent laboratory demonstrations have shown 170 Gb/in^2.

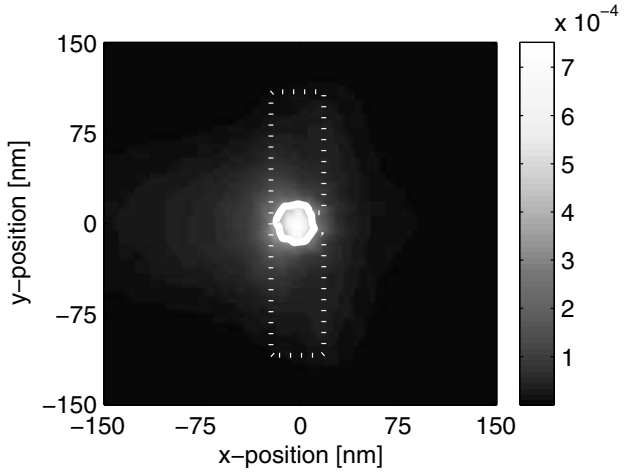

FIG. 6. Dissipated power density (mW/nm^3) on the top surface of the media when the ridge waveguide is placed 30 nm under a SIL. The FWHM contour is emphasized with a thick white line. Projection of the boundaries (dotted white contour) of the ridge waveguide is added to the figure to illustrate the relative position of the hot spot with respect to the optical transducer.

To the best of our knowledge, this is the first optical system that predicts such a high transmission efficiency in a small optical spot well beyond the diffraction limit. There have been other optical systems that produce similarly sized optical spots, especially apertureless configurations. However, the optical system in this study provides a significantly higher transmission efficiency compared to previous optical systems. Although we discussed possible implications for data storage in the previous paragraph, the results can attract wide-ranging interest from the community that uses localized surface plasmons.

From a broader perspective, this result points to another interesting finding. The optimum air thickness, 30 nm, is significantly thinner than the optimum for a typical Otto configuration, which is on the order of 300–400 nm. To excite surface plasmons in a typical Otto configuration, collimated light is used to illuminate the structures, which has a single component in the **k** spectrum. The focused light obtained from a SIL, on the other hand, has a wide **k** spectrum distribution. We found that the difference of the results in Fig. 5 from the previous expectations is a result of the difference in the **k** spectrum of the incident electric field. Therefore, this result points out that the interaction of surface plasmons and the optimum geometries to excite surface plasmons are different for collimated and focused light.

The focused light obtained from a SIL has a wide **k** spectrum, which can be viewed as a summation of

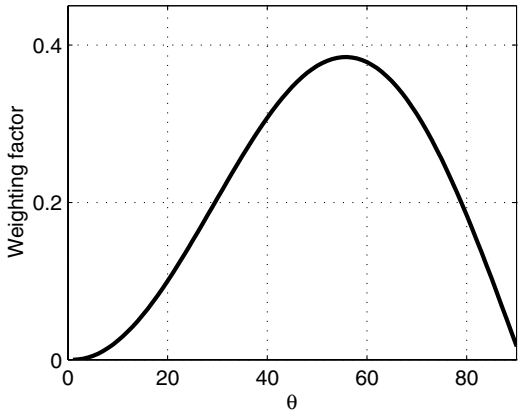

FIG. 7. Weighting factor of each plane wave component in a SIL.

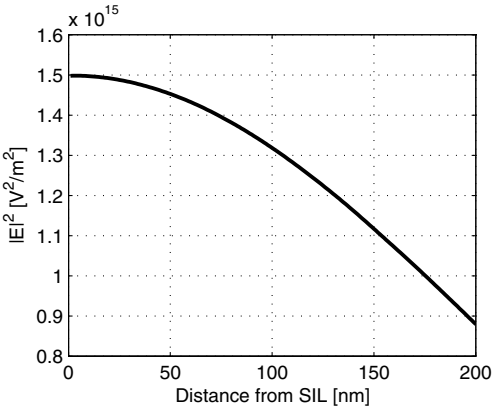

FIG. 8. Decay of the fields due to the defocusing of the SIL.

weighted plane wave components. Equation (1) is a summation of plane waves propagating in the **k** direction with an amplitude of $\frac{1}{\lambda}\sin\theta\sqrt{\cos\theta}$. Therefore, the power density of the **k** spectrum is scaled by $\sin^2\theta\cos\theta$ in a SIL, as shown in Fig. 7. Using an analytical model the reflectivity of the film can be calculated to find out the surface plasmon resonance (SPR) of the film stack. We found that the SPR angles are 46.9°, 34.3°, 32.3°, and 31.9°, for $L = 30$, 100, 200, and 300 nm, respectively. The weighting factor in Fig. 7 has a maximum around 55°, which favors the larger SPR angle of the film stack with a thinner dielectric layer. In addition, we found out that the absorption by the silver film at the resonance angle for the film stack with a thinner dielectric layer is not as large, but the angular spectrum of the resonance is much broader. The integration of the broader but weaker spectrum of the film stack with a thinner dielectric layer yields higher values.

Another factor that impacts the interaction of focused light with surface plasmons, and, therefore, the results in Fig. 5, is the reduction of the incident field amplitude due to defocusing of the SIL. Beneath the SIL the size of the optical spot enlarges quickly with increasing distance. The amplitude of the electric field decreases correspondingly. As the observation plane gets farther away from the SIL surface, the size of the focused spot increases. The increase of the spot size reduces the incident field amplitude. Figure 8 illustrates the reduction of the fields due to the defocusing of the SIL. Figure 8 gives higher values for smaller distances from the bottom SIL surface. This suggests that a higher incident field amplitude is expected on the transducer surface for a film stack with a thinner dielectric layer, which causes stronger near-field radiation.

In summary, the interaction of surface plasmons and the optimum geometries to excite surface plasmons is different for collimated and focused light. Scaling and integration of the **k** spectrum of the focused light and defocusing of the optical device impact this interaction and near-field radiation of the transducer. We also reported an optical device that provides a high transmission efficiency in a small spot well beyond the diffraction limit. The enhancement of the near-field radiation from the optical transducer was obtained by placing it in the vicinity of a SIL. There are two reasons for the enhancement: (1) placing the near-field transducer in the proximity of a SIL increases the incident electric field over the transducer, and (2) placing a low refractive index material between the SIL and ridge waveguide transducer creates evanescent fields which couple efficiently into the surface plasmon modes over the metal film.

This work was performed as part of the INSIC HAMR ATP Program, with the support of the U.S. Department of Commerce, National Institute of Standards and Technology, Advanced Technology Program, Cooperative Agreement No. 70NANB1H3056.

*Electronic address: kursat.sendur@gmail.com

[1] S. M. Mansfield and G. S. Kino, Appl. Phys. Lett. **57**, 2615 (1990).
[2] A. Hartschuh *et al.*, Phys. Rev. Lett. **90**, 095503 (2003).
[3] R. D. Grober, R. J. Schoelkopf, and D. E. Prober, Appl. Phys. Lett. **70**, 1354 (1997).
[4] C. Mihalcea *et al.*, Appl. Phys. Lett. **68**, 3531 (1996).
[5] M. Ohtsu and H. Hori, *Near-Field Nano-Optics* (Kluwer Academic, New York, NY, 1999).
[6] W. A. Challener *et al.*, Jpn. J. Appl. Phys. **42**, 981 (2003).
[7] P. L. Lu and S. H. Charap, J. Appl. Phys. **75**, 5768 (2001).
[8] X. Shi, R. Thornton, and L. Hesselink, Proc. SPIE Int. Soc. Opt. Eng. **4342**, 320 (2001).
[9] X. Shi and L. Hesselink, Jpn. J. Appl. Phys. **41**, 1632 (2001).
[10] T. E. Schlesinger *et al.*, Jpn. J. Appl. Phys. **41**, 1821 (2002).
[11] E. X. Jin and X. Xu, Jpn. J. Appl. Phys. **43**, 407 (2004).
[12] A. V. Itagi *et al.*, Appl. Phys. Lett. **83**, 4474 (2003).
[13] K. Sendur, W. Challener, and C. Peng, J. Appl. Phys. **96**, 2743 (2004).
[14] W. Challener, K. Sendur, and C. Peng, Opt. Express **11**, 3160 (2003).
[15] A. Otto, Z. Phys. **216**, 398 (1968).
[16] E. Wolf, Proc. R. Soc. London A **253**, 349 (1959).
[17] B. Richards and E. Wolf, Proc. R. Soc. London A **253**, 358 (1959).
[18] All the FEM calculations in this report are performed with HFSS™ from Ansoft Inc.
[19] E. D. Palik, *Handbook of Optical Constants of Solids* (Academic Press, San Diego, CA, 1998).